



Study of B_s Oscillations with the ALEPH detector at LEP^{1,2}

Gaëlle Boix

Universitat Autònoma de Barcelona
Departament de Física
Institut de Física d'Altes Energies
Edifici Cn E-08193 Bellaterra (Barcelona)

and

CERN EP-Division ALE
CH-1211 Geneva 23

June 2001

¹PhD. Dissertation.

²Work supported by the Commission of the European Communities, contract ERBFMBICT982894.

Contents

1	Introduction	1
2	Flavour Physics and B-Mixing in the Standard Model	3
2.1	Cabbibo-Kobayashi-Maskawa (CKM) Matrix	4
2.1.1	Estimation of CKM elements	5
2.1.2	CKM matrix and CP Violation	7
2.2	Phenomenology of B mixing and oscillations	9
2.2.1	B mixing and the CKM matrix	11
2.2.2	B mixing and CP violation	14
2.2.3	State-of-the-art	15
2.3	B mixing beyond the Standard Model	16
3	Experimental Method	19
3.1	Basic features of a B mixing measurement	20
3.1.1	Proper time measurement	23
3.1.2	Flavour tagging	24
3.1.3	Signal enrichment and background evaluation	26
3.1.4	Effect of mistag, background, and resolution	26
3.2	Fitting procedure	28
3.3	The amplitude method	29
3.3.1	Interpretation	30
3.3.2	The amplitude analysis	33
3.3.3	The toy experiments	42
3.3.4	The estimate of the significance	46
3.3.5	Sensitivity limiting factors	52
4	Experimental Setup	55
4.1	The LEP Storage Ring	55
4.2	The ALEPH Detector and Performance	58
4.2.1	The tracking system	60
4.2.2	Calorimetry	63
4.2.3	Energy flow	65
4.2.4	Luminosity measurement	66

5	General analysis tools	69
5.1	Hadronic selection	69
5.2	Jet algorithms	70
5.2.1	The JADE algorithm	70
5.2.2	The Nucleated jet algorithm	71
5.2.3	A cone algorithm: BTCONE	71
5.3	Lepton identification	71
5.3.1	Electron identification	72
5.3.2	Muon identification	74
5.4	Primary vertex finding	75
5.5	Impact parameter	77
5.6	Inclusive secondary vertex finders	78
5.6.1	QVSRCH	78
5.6.2	VNFIT	78
5.7	General b tagging	80
5.7.1	QIPBTAG	80
5.7.2	QVSRCH	81
5.7.3	Mass tag: QBMTAG	81
6	Inclusive semileptonic event selection	85
6.1	Data and simulation samples	86
6.2	Data sample pre-selection	86
6.3	Vertex algorithm and selection	87
6.3.1	Search for a seed	88
6.3.2	The c track selection	88
6.3.3	Photon recovery	92
6.3.4	The “B track”	93
6.3.5	Global b-vertex fit	94
6.3.6	The decay length	94
6.3.7	Vertex selection and class definition	94
6.3.8	The bias and pull correction	95
6.4	The b-hadron enrichment	98
6.5	The $b \rightarrow \ell$ enrichment	103
6.6	Final selection	108
6.7	Proper time measurement	110
6.7.1	Momentum measurement	110
6.7.2	Proper time	114
6.7.3	Proper time efficiency	114
6.8	Kaon identification	116
6.8.1	Charged kaons	116
6.8.2	Neutral kaons	117
6.9	B_s enrichment	121
6.10	Initial state tag	128
6.10.1	Opposite hemisphere	129
6.10.2	Same hemisphere	131
6.10.3	Flavour tag performance	136

7	Supplementary B_s selections	139
7.1	Selection of $D_s \ell$ pairs	139
7.1.1	Sample composition	140
7.1.2	Event characterization	141
7.2	Selection of exclusive hadronic flavour final states	142
7.2.1	Sample composition	143
7.2.2	Event characterization	144
7.3	Flavour tagging	145
7.3.1	Final state tag	145
7.3.2	Initial state tag	145
8	Results on B_s Oscillations	147
8.1	The Δm_s fit	147
8.1.1	Input description	148
8.1.2	Results on the inclusive semileptonic event sample	149
8.2	Systematic uncertainties	153
8.3	Final result for the inclusive semileptonic sample	156
8.4	Checks	157
8.4.1	Checks with simulated events	157
8.4.2	Impact of the uncertainty treatment	160
8.5	Results with supplementary event selections	161
8.6	Combination with other results	164
8.6.1	Combination with other ALEPH results	164
8.6.2	World combination	164
8.6.3	Interpretation	166
9	Conclusions	169

List of Figures

2.1	Unitarity triangle in the complex $(\bar{\rho}, \bar{\eta})$ plane.	9
2.2	Feynman diagrams for B mixing.	12
2.3	Probability density function for Δm_s	14
3.1	Event discovery for B mixing from the ARGUS Collaboration.	21
3.2	Proper time distribution for mixed/unmixed B_d and B_s mesons.	22
3.3	Semileptonic B^0 meson decay diagrams.	24
3.4	Cascade B^0 meson decay diagrams.	25
3.5	Cascade $b \rightarrow \bar{c} \rightarrow \ell$ decay diagram.	25
3.6	B_s oscillations signal resolution as a function of analysis parameters.	27
3.7	Winter 1999 world average amplitude plot.	31
3.8	Likelihood derived from the winter 1999 combined amplitudes.	32
3.9	Reconstructed proper time distributions for the oscillating component.	34
3.10	Expected amplitude values.	36
3.11	Amplitude shape for a signal at $\Delta m = 0.5 \text{ ps}^{-1}$	38
3.12	Expected shapes of Fourier spectra.	39
3.13	Probability contours in the $(\overline{\Delta\mathcal{L}}, \omega)$ plane.	41
3.14	Parameter optimization for the toy events generation.	44
3.15	Typical proper time efficiency shape.	45
3.16	Amplitude uncertainties comparison.	45
3.17	Expected amplitude and uncertainty for type S samples.	46
3.18	Point-to-point fluctuations for four sets of samples.	48
3.19	Minima of $\Delta\mathcal{L}$ for 2000 samples of type S	49
3.20	Minima of $\Delta\mathcal{L}$ for 2000 samples of type S'	50
3.21	Average amplitude and expected uncertainty for a signal at $\Delta m_s = 14.8 \text{ ps}^{-1}$	51
3.22	Minima of $\Delta\mathcal{L}$ for 2000 samples of type S' with $\Delta m_s = 150 \text{ ps}^{-1}$	51
3.23	Proper time resolution effect on the amplitude uncertainty.	53
3.24	Effect of the decay length resolution treatment on the amplitude uncertainty.	54
4.1	Schematic view of LEP and the Surrounding Area.	56
4.2	CERN Accelerators, LEP injection chain.	57
4.3	LEP Integrated luminosity from 1989 to 2000.	58
4.4	Schematic view of the ALEPH Detector.	59
4.5	Configuration of the vertex detector.	60
4.6	Time projection chamber overall view.	62
4.7	Material before the electromagnetic calorimeter.	63
4.8	Overall geometry of the HCAL surrounding the magnet and the ECAL.	64

5.1	The ECAL estimators for electron candidates.	73
5.2	Muon identification estimators.	75
5.3	Primary vertex finder projection	76
5.4	Impact parameter definition.	77
5.5	Decay length resolution for b-hadrons using QVSRCH or VNFIT.	79
5.6	Decay length reconstruction efficiency comparison for QVSRCH and VNFIT.	80
5.7	QIPBTAG estimator for $Z \rightarrow uds$ and $Z \rightarrow b\bar{b}$ simulated events.	82
5.8	QVSRCH b-tagging estimator distribution for uds and $b\bar{b}$ events.	82
5.9	QBMTAG estimator distribution for uds and b hemispheres.	83
6.1	Semileptonic B_s decay schematic.	87
6.2	Distribution of the discriminant variables for the track separation-1.	90
6.3	Distribution of the discriminant variables for the track separation-2.	90
6.4	Distribution of the discriminant variables for the track separation-3.	91
6.5	Track separation neural network output in VNFIT events.	91
6.6	Decay length resolution for two vertex classes.	97
6.7	Decay length bias wrt reconstructed decay length.	97
6.8	Decay length distribution for all selected events.	98
6.9	Decay length pull distribution before and after correction.	99
6.10	Lepton variables used for b-tagging.	100
6.11	QIPBTAG variables used for b-tagging.	100
6.12	QBMTAG variables used for b-tagging.	101
6.13	QVSRCH variables used for b-tagging.	101
6.14	Combined b-tagging variable distribution.	102
6.15	Comparison of b-tagging performance.	102
6.16	Schematic of the boost effect on $b \rightarrow \ell$ and $b \rightarrow c \rightarrow \ell$ events.	104
6.17	Lepton impact parameter wrt the charm vertex.	105
6.18	Lepton variables used for $b \rightarrow \ell$ enrichment.	105
6.19	Shape variables used for $b \rightarrow \ell$ enrichment.	106
6.20	Jet charged energy and lepton energy in the (ℓ D) rest frame.	106
6.21	Lepton impact parameter significance and neutrino energy.	107
6.22	Combined $b \rightarrow \ell$ enrichment variable distribution.	108
6.23	Comparison of $b \rightarrow \ell$ enrichment performance.	109
6.24	$b \rightarrow \ell$ purity as a function of N_{bltag}	109
6.25	Distribution of events among the vertex classes.	111
6.26	Average neutrino energy bias on $b \rightarrow \ell$ Monte Carlo.	112
6.27	Momentum bias wrt the neutrino energy.	113
6.28	Relative momentum bias, before and after average-bias correction.	113
6.29	Relative momentum resolution for two classes	114
6.30	Proper time distribution in the selected sample.	115
6.31	Distribution of the uncertainty on the proper time in the selected sample.	115
6.32	Proper time efficiency for $B_s \rightarrow \ell$ Monte Carlo.	116
6.33	Combined charged kaon estimators.	117
6.34	K_S reconstructed mass and distance of flight.	118
6.35	The χ^2 of the two decay pions with the primary vertex.	119
6.36	χ^2 of the K_S mass constraint fit, and K_S momentum.	119
6.37	Angular estimators for K_S candidates.	120
6.38	Combined neutral kaon estimators.	120

6.39	Charm vertex charge and multiplicity.	122
6.40	Charm vertex weighted charge multiplicity and momentum.	123
6.41	Fragmentation kaon estimators.	123
6.42	Charged decay kaon estimators.	124
6.43	Neutral decay kaon estimators.	125
6.44	Invariant ϕ mass and track separation estimators.	125
6.45	Combined enrichment variable.	126
6.46	Charm vertex charge and multiplicity (corrected).	127
6.47	Charm vertex weighted charge multiplicity and momentum (corrected).	127
6.48	Combined enrichment variable (corrected).	128
6.49	b-hadron species probabilities as a function of N_{enrich}	129
6.50	Opposite side initial state tag variable.	131
6.51	Weighted primary vertex charge with $\kappa = 0$	132
6.52	Weighted primary vertex charge with $\kappa = 0.6$	133
6.53	Weighted primary vertex charge with $\kappa = 1$	133
6.54	Primary vertex charge, c tracks excluded, with $\kappa = 0$	134
6.55	Primary vertex charge, c tracks excluded, with $\kappa = 0.3$	134
6.56	Charged fragmentation kaon estimator.	135
6.57	Signed thrust polar angle.	135
6.58	Initial state tag combined variable.	136
6.59	Calibration of the Initial State tag variable for $B_s \rightarrow \ell$ events.	137
6.60	Calibration of the N_{is} variable for other hadrons.	137
7.1	Reconstructed mass spectra for the D_s selected sample.	141
7.2	Mass spectra for the B_s hadronic hadronic final states.	144
8.1	Proper time distribution for $u\bar{u}$, $d\bar{d}$, $s\bar{s}$ and charm background.	149
8.2	Probability distribution for all sample components.	150
8.3	Mistag probability distribution for all b-hadron species.	151
8.4	Likelihood function in the inclusive semileptonic data sample.	152
8.5	Amplitude spectrum for the inclusive semileptonic sample (stat).	153
8.6	Primary vertex reconstruction on light-quark events.	155
8.7	Amplitude spectrum for the inclusive semileptonic sample.	156
8.8	Amplitude spectrum for the <i>previous</i> inclusive semileptonic sample.	157
8.9	Likelihood function in a sample of B_s simulated events.	158
8.10	Amplitude spectrum for a sample of B_s simulated events.	158
8.11	Likelihood function in a sample of $q\bar{q}$ simulated events.	159
8.12	Amplitude spectrum for a sample of $q\bar{q}$ simulated events.	159
8.13	Amplitude uncertainty using average decay length uncertainties.	160
8.14	Amplitude spectrum for the $D_s \ell$ event selection.	161
8.15	Likelihood function in the $D_s \ell$ data sample.	162
8.16	Amplitude spectrum for the selection of exclusive B_s decays.	162
8.17	Amplitude uncertainty for the three event selections.	163
8.18	ALEPH combined amplitude spectrum.	165
8.19	ALEPH combined likelihood function for Δm_s	165
8.20	Comparison of the statistical uncertainty of all B_s results in the World.	166
8.21	Amplitude spectrum for the world combination.	167
8.22	World combined likelihood function for Δm_s	167

8.23	Display of a $D_s \ell$ candidate.	168
9.1	Evolution of the ALEPH B_s oscillation results.	170

List of Tables

4.1	Momentum and impact parameter resolution.	63
6.1	Definition of the vertex classes.	96
6.2	Sample composition after the lepton and vertex selections.	98
6.3	Sample composition after the lepton, the vertex, and the b-tagging selections.	103
6.4	Performance of the $b \rightarrow \ell$ enrichment on $Z \rightarrow b\bar{b}$	108
6.5	Final Sample composition.	110
7.1	Sample composition for the $D_s \ell$ selection.	140
7.2	Event selection efficiencies for each channel.	143
7.3	Sample composition for the B_s exclusive reconstruction.	145
8.1	Systematic uncertainties for the inclusive semileptonic analysis.	154
8.2	Physical inputs to the B_s oscillation fit.	155

Chapter 1

Introduction

The Standard Model [1, 2], since its first formulation, has had an enormous phenomenological success, with most of its predictions confirmed by experimental results. However, several questions are still unanswered. For instance, it is not understood why there are three and only three fermion families, the pattern of masses and mixings cannot be explained, the origin of the Standard Model flavour structure is still mysterious, etc. These questions, among others, are presently studied both by theorists and experimentalists in particle physics. In this thesis the quark mixing part of the Standard Model, with the CKM matrix [3, 4], is addressed.

The CKM matrix elements are interesting to be studied on their own, as fundamental parameters of the Lagrangian of the Standard Model. One of the major goals of these studies is to understand the phenomenon of CP violation. The violation of CP is one of the three necessary ingredients to generate the observed excess of matter over antimatter in the universe [5]. However, the amount of CP violation which can be generated by the Standard Model appears to be orders of magnitude below what cosmological observations require [4, 6]. This argument gives strong motivation to search for new physics in that context.

Many experiments are currently studying physical observables in which CP violation would be visible, both with kaons and B mesons. However, insights into CP violation may also be provided by CP conserving experiments. One of the major measurements in this respect is the mixing of neutral B mesons, B_d and B_s , and consequently the determination of the $|V_{td}|$ and $|V_{ts}|$ CKM matrix elements. These two elements are, up to now, only accessible through flavour changing neutral current processes like B mixing. Their accurate measurement is important to test the unitarity of the CKM matrix. Moreover, physics beyond the Standard Model could be revealed with the measurement of the B mixing parameters [7].

The mass difference between B_d and \bar{B}_d (Δm_d) is now measured with few percent relative accuracy [8]. As of today, no precise measurement of Δm_s is available. The ALEPH experiment at LEP has greatly contributed to the overall present knowledge of B_s oscillations. Together with the other LEP experiments, ALEPH has collected the data sample in which the largest number of B_s decays can be reconstructed. The detector performance on charged and neutral particle momentum measurement, secondary vertex reconstruction and particle identification are adequate for B_s oscillation studies.

When I started my work on B_s oscillations, a first hint for an oscillation signal seemed to be appearing from the world combination, but no clear method existed to estimate the probability that this hint originate from a statistical fluctuation. My first contribution was a detailed study [9] of the amplitude method. Analytical expressions for the expected shape of the amplitude were derived and a procedure making use of toy experiments was proposed as a tool to estimate the significance of a possible oscillation signal.

At that time, the single most sensitive B_s oscillations analysis was the ALEPH study with an inclusive semileptonic event sample [10]. The ALEPH data taken at energies close to the Z mass had just been reprocessed and some of the published analyses were being revisited to profit from the improved reconstruction. A critical study of Ref. [10] showed that room for improvement existed beyond the gain from the reprocessing, and encouraged me to perform a new B_s oscillation analysis with an inclusive semileptonic event sample in ALEPH. The main item for which improvement was understood to be possible was the reconstruction of the B meson decay length. However, all the other relevant ingredients were studied in detailed and significantly improved. As a result, the sensitivity of the analysis was sizeably increased. The precision on the measured amplitude at high frequency was improved by more than a factor of two. A hint for a Δm_s measurement, with a statistical significance of ~ 1.5 standard deviations, was obtained with the analysis in Ref. [10]. The new analysis confirmed the hint with a significance increased to slightly more than two standard deviations.

This thesis dissertation is organized as follows. The theoretical framework for B_s oscillations, the CKM matrix, and their connection with CP violation are revised in Chapter 2. The experimental method for B mixing and oscillation studies, together with a detailed discussion on the amplitude method are the subject of Chapter 3. In Chapter 4, the LEP collider and the ALEPH detector are briefly described. Those analysis tools used for the data analysis but not developed by myself are presented in Chapter 5. The core of this thesis is developed in Chapter 6: it contains the description of the inclusive semileptonic event sample selection for the B_s oscillation study. Two complementary selections of event samples enriched in B_s mesons are presented in Chapter 7. The results on B_s oscillations obtained with the three event samples described in this thesis are provided in Chapter 8. The ALEPH combination and the world combination are also presented. Finally, the conclusions are given in Chapter 9.

Chapter 2

Flavour Physics and B-Mixing in the Standard Model

Particle physics has a well established theoretical framework which has been successful for many years: the Standard Model [1, 2]. This model explains and includes basically all the experimental observations made so far, in particular high precision tests, at the per-mil level, which have been performed in the past decade. However, many parameters in the model are not predicted by the theory, and have to be measured experimentally. The particles (or fields) of the Standard Model are divided into gauge fields associated with the gauge groups, and matter fields. All matter fields are fermions of two types distinguished by the kind of interactions they are sensitive to; these particles are quarks and leptons. They appear in three families (or generations) each containing two quarks and two leptons. The families all have the same interactions with the gauge fields; only their masses (and couplings to the Higgs field) are different. It is common to use the term *flavour* to denote the different particles and therefore to say u-flavour, or b-flavour.

The flavour sector of the model studies fermion masses and mixings, and is, at present, one of the least well tested. Several of its relevant parameters, in particular quark mixing, are only known to an accuracy of $\mathcal{O}(30\%)$, while other parameters of the model, in the electroweak sector, are measured with a precision of one percent or even better, and allow a fine test of the Standard Model. The so-called flavour parameters are 13: six quark masses, four parameters related with quark mixing, and in the lepton sector, assuming massless neutrinos, three charged lepton masses. If neutrinos are proved to be massive, three new masses and a set of mixing parameters should be added.

Some of the remaining open questions in the Standard Model are related with the flavour parameters, hence the interest of improving their experimental knowledge. The flavour parameters exhibit a “family hierarchy”, *i.e.*, their relative magnitude depends on the family. No theoretical explanation exists for this hierarchy, the phenomenon is called *flavour puzzle*. The strength of flavour changing neutral current processes (FCNC) depends on the flavour parameters. The phenomenon of CP violation is also closely related to flavour physics and it is one of the least tested aspects of the Standard Model. Most of the theoretically proposed extensions of the Standard Model predict new sources for CP violation, and some for FCNC as well. These reasons make important the study of flavour physics inside the Standard

Model, and maybe beyond.

Particle-antiparticle mixing happens in neutral meson systems which are not auto-conjugated (the π^0 meson, for instance, being its own antiparticle, does not mix). Two B mesons have this property: B_d and B_s . From the experimental point of view, the two neutral B mesons have very distinct mixing properties. The B_d system has already been deeply studied. The focus of this thesis is devoted to the B_s system whose experimental knowledge is far behind.

The flavour structure of the Standard Model is presented in the first Section of this Chapter. Stress is put on the aspects still to be understood or measured, and in particular on the Cabbibo-Kobayashi-Maskawa (CKM) matrix [3, 4] which describes the quark mixing. The present state-of-the-art is given with a brief review of methods already used to measure some of the matrix elements. A very brief introduction to CP violation in the Standard Model, which arises from the CKM matrix structure with three families, follows.

The phenomenology of neutral mesons mixing is introduced in Section 2.2. Although the experimental focus of the present thesis is on B_s oscillations, both B_d and B_s are included in the theoretical discussion. Stress is put on the differences between them and their importance from the experimental point of view. A discussion on how B_s mixing is related to some of the elements of the CKM matrix and CP violation is given, as well as the present state-of-the-art.

Finally, some of the possible extensions to the Standard Model are very briefly presented with their implications on neutral B-meson mixing.

2.1 Cabbibo-Kobayashi-Maskawa (CKM) Matrix

In the Standard Model, only the charged current sector, with exchange of a W-boson, can accommodate family and flavour-changing transitions. The interaction Lagrangian density responsible for these transitions in the quark sector, is written

$$\mathcal{L}_{CC} = \frac{g}{2\sqrt{2}} \sum_{i,j} [\bar{u}_i \gamma^\mu (1 - \gamma^5) V_{ij} d_j] W_\mu^+ + h.c. \quad (2.1)$$

where V_{ij} are terms of the Cabbibo-Kobayashi-Maskawa (CKM) matrix, and the indices i and j run over the three quark families.

The CKM matrix V_{CKM} is a rotation from the quark mass eigenstates, d, s, and b, to a set of different states d' , s' , and b' , the weak eigenstates. Therefore, if no other quark families exist, the 3×3 CKM matrix should be unitary. A common representation is

$$\begin{pmatrix} d' \\ s' \\ b' \end{pmatrix} = \begin{pmatrix} V_{ud} & V_{us} & V_{ub} \\ V_{cd} & V_{cs} & V_{cb} \\ V_{td} & V_{ts} & V_{tb} \end{pmatrix} \begin{pmatrix} d \\ s \\ b \end{pmatrix}. \quad (2.2)$$

To a first order approximation, the CKM matrix is simply the identity matrix, so that the dominant transitions are inside a single family: $u \rightarrow d$, $c \rightarrow s$, $t \rightarrow b$. Family-changing transitions between quarks through a W^\pm -gauge boson are made possible by the fact that none of the off-diagonal elements is exactly zero. These off-diagonal elements of the matrix can therefore be measured through the experimental study of the family-changing transitions. These transitions occur in some mesons decays, in FCNC processes, as well as in the CP violation inside the Standard Model and constitute the main interest of flavour physics.

2.1.1 Estimation of CKM elements

The values of the CKM matrix elements are, like the fermion masses, fundamental input parameters of the Standard Model. Experimental measurements are needed in order to give insights into their values.

An intense experimental effort is being made to measure the CKM elements. They can be determined basically in three ways, with direct measurements of Standard Model tree-level processes, with indirect measurements of Standard Model loop processes, or applying unitarity, *i.e.*, using some of the relations from $V_{\text{CKM}}V_{\text{CKM}}^\dagger = 1$.

The present knowledge of the matrix elements comes from the following sources:

- $|V_{\text{ud}}|$

Three different methods exist to measure $|V_{\text{ud}}|$. *Nuclear superallowed Fermi beta decays*: the method consists of comparing the rate of nuclear beta decays of spin 0^+ and isospin 1 states to that of the muon. This rate is proportional to $|V_{\text{ud}}|^2$. The measurement is performed with several nuclei and the average is taken. This method is, at present, the most precise, but it is limited by the uncertainty on the theoretical corrections, especially on nucleus dependent corrections. The result obtained with this method is $|V_{\text{ud}}| = 0.9740 \pm 0.0005$ [11]. *Neutron decay*: $|V_{\text{ud}}|$ is in this case extracted from the neutron lifetime measurement. The limiting factor is the experimental uncertainty on g_A/g_V . One of the available values is $|V_{\text{ud}}| = 0.9790 \pm 0.0017$ [12]. *Pion beta decay*: it is the cleanest method from the theoretical point of view. However, the branching ratio for the process $\pi^+ \rightarrow \pi^0 e^+ \nu_e$ is only of the order of 10^{-8} , and therefore it is limited from the experimental side. The present value obtained is $|V_{\text{ud}}| = 0.9679 \pm 0.0161$ [11]. The theoretical uncertainty estimates of the above results are controversial and so is the global average value of $|V_{\text{ud}}|$. The present value quoted in the PDG (Particle Data Group) is: $|V_{\text{ud}}| = 0.9735 \pm 0.0008$ [13].

- $|V_{\text{us}}|$

Mainly two ways are exploited to determine $|V_{\text{us}}|$. *K_{e3} decays*: these decays are: $K^+ \rightarrow \pi^0 e^+ \nu_e$ and $K_L^0 \rightarrow \pi^- e^+ \nu_e$. Chiral perturbation theory is used to extract the value of $|V_{\text{us}}|$ from the measured K_{e3} decay rates. The present estimated value reads $|V_{\text{us}}| = 0.2196 \pm 0.0023$, Ref. [14]. *Semileptonic hyperon decays*: in this case the $|V_{\text{us}}|$ extraction is dominated by large theoretical uncertainties. The best value quoted in the PDG [13] with this method is $|V_{\text{us}}| = 0.2176 \pm 0.0026$, but the value obtained from K_{e3} decays is recommended for use.

- $|V_{\text{cd}}|$

The value of $|V_{\text{cd}}|$ can be obtained from single charm production in deep inelastic neutrino (antineutrino)-nucleon scattering, supplemented by measurements of semileptonic branching fractions of charmed mesons. The present average is: $|V_{\text{cd}}| = 0.224 \pm 0.016$ [13].

- $|V_{\text{cs}}|$

The value of $|V_{\text{cs}}|$ used to be obtained in a similar manner as for $|V_{\text{us}}|$, from D_{e3} decays, by comparing the data with the theoretical decay width. This method uses model-dependent form-factors which introduce an important uncertainty in the final

result, which reads $|V_{cs}| = 1.04 \pm 0.16$ [13]. Recent measurements from the ALEPH, DELPHI, and OPAL Collaborations [15] of the inclusive charm production rate in W-boson decays, $R_c^W = \Gamma(W \rightarrow cX)/\Gamma(W \rightarrow \text{hadrons})$, allow a more precise value to be extracted, $|V_{cs}| = 0.95 \pm 0.08$ [16], which is compatible with the one previously quoted. No average of these two numbers is provided by the PDG.

- $|V_{cb}|$

The heavy quark effective theory (HQET) [17] provides a nearly model-independent treatment of B semileptonic decays to charmed mesons, assuming that both the b and c quarks are heavy enough for the theory to apply. The matrix element $|V_{cb}|$ can be determined from B semileptonic decays studies in the HQET framework [18]. There are two experimental methods to obtain $|V_{cb}|$: the *inclusive* method, which uses the semileptonic decay width of b-quark decays, and the *exclusive* method, where $|V_{cb}|$ is extracted by studying the exclusive $\bar{B}^0 \rightarrow D^{*+} \ell^- \bar{\nu}_\ell$ decay. The latest result from LEP with the inclusive method, $|V_{cb}| = 0.04070 \pm 0.00050_{(\text{exp})} \pm 0.00204_{(\text{th})}$, is largely dominated by the theoretical uncertainties but it is more precise than the exclusive one, $|V_{cb}| = 0.0398 \pm 0.0018_{(\text{exp})} \pm 0.0022_{(\text{th})}$ [19]. The LEP average, $|V_{cb}| = 0.0404 \pm 0.0018$, can be compared to the average from similar measurements performed at CLEO: $|V_{cb}| = 0.0404 \pm 0.0034$ [13]. No clear procedure to average LEP and CLEO results exist and therefore no average is provided by the PDG.

- $|V_{ub}|$

Until now, three different methods have been used to measure $|V_{ub}|$. *Endpoint*: at CLEO, with data at the $\Upsilon(4S)$ resonance, the decay of $b \rightarrow u \ell \bar{\nu}$ is measured from the lepton energy spectrum above the endpoint of the $b \rightarrow c \ell \bar{\nu}$ spectrum. *Exclusive*: decays such as $B \rightarrow \pi \ell \bar{\nu}_\ell$ and $B \rightarrow \rho \ell \bar{\nu}_\ell$, sensitive to $|V_{ub}|$ are accessible at CLEO. These two methods are, however, limited by theoretical model dependences. *Inclusive*: at LEP the charmless semileptonic B branching fraction can be determined by discriminating $b \rightarrow u$ from $b \rightarrow c$ decays. The value of $|V_{ub}|$ is then extracted from the measured branching fraction. The latest LEP average available gives $|V_{ub}| = (4.13_{-0.47}^{+0.42}(\text{stat+exp}) \pm 0.43_{(\text{b} \rightarrow \text{c syst})} \pm 0.24_{(\text{b} \rightarrow \text{u syst})}) \pm 0.20_{(\text{HQET})} \times 10^{-3}$ [20]. The CLEO Collaboration has produced an average of their results which can be compared to that of LEP and reads, $|V_{ub}| = (3.25 \pm 0.14_{(\text{stat})} \pm 0.55_{(\text{syst})}^{+0.21} \pm 0.55_{(\text{theo})}) \times 10^{-3}$ [21]. No average of these results is provided by the PDG.

- $|V_{tb}|$

No measurement of the $|V_{tb}|$ matrix element has been performed without the assumption of unitarity of the CKM matrix and three quark generations in the Standard Model until now. The ratio $BR(t \rightarrow Wb)/BR(t \rightarrow Wq)$, where q is a down-type quark, can be measured with the $t\bar{t}$ data collected at the Tevatron. This measurement, with the above assumptions, allows a value of $|V_{tb}|$ to be extracted: $|V_{tb}| = 0.99 \pm 0.15$ [22]. A more accurate, and less model-dependent, estimate is expected using the single top production cross-section with data from the second phase of the Tevatron accelerator at Fermilab. It is also possible to extract the value of $|V_{tb}|$ from electroweak loop corrections without assuming unitarity, the value obtained is $|V_{tb}| = 0.77_{-0.24}^{+0.18}$ [23].

- $|V_{ts}|$ and $|V_{td}|$

These two matrix elements are not measured directly at present. Their value can be

estimated from top quark loop correction to some processes (*e.g.* $b \rightarrow s\gamma$), they are also closely related to the B meson mixing, as explained later in Section 2.2.1.

Some comments

If the CKM matrix is unitary, its elements in the first row (Eq. 2.2) should verify $|V_{ud}|^2 + |V_{us}|^2 + |V_{ub}|^2 = 1$. If the values of the matrix elements quoted above are taken, a discrepancy of more than one and a half standard deviations from unitarity is obtained: $|V_{ud}|^2 + |V_{us}|^2 + |V_{ub}|^2 = 0.9959 \pm 0.0025$; the discrepancy is larger, 0.9955 ± 0.0020 , if the second value of $|V_{us}|$ is taken instead of the first. Although not felt as a real problem yet [11, 13], it gives strong motivation for pursuing on the $|V_{ud}|$ and $|V_{us}|$ estimates, both from the experimental and theoretical sides. The element $|V_{ub}|$ has the biggest relative uncertainty of the three, however, it is intrinsically too small to make a difference on the unitarity test. A definite deviation from unitarity would be proof of the existence of physics beyond the Standard Model.

Within the Standard Model, all branching fractions of the W-boson depend, at tree level, on the six matrix elements $|V_{qq'}|$ not involving the top quark. The semileptonic branching ratio of the W-boson is inversely proportional to the squared sum of these six matrix elements,

$$1/BR(W \rightarrow \ell\bar{\nu}_\ell) = 3\{1 + [1 + \alpha_s(M_W^2)/\pi] \sum_{i=u,c,j=d,s,b} |V_{ij}|^2\} \quad (2.3)$$

where α_s is the strong coupling constant. Taking the experimental values quoted above for $|V_{ud}|$, $|V_{us}|$, $|V_{ub}|$, $|V_{cd}|$, and $|V_{cb}|$, an estimate for $|V_{cs}|$ can be extracted: $|V_{cs}| = 0.989 \pm 0.016$, as in Ref. [16], which is much more precise than the direct measurement obtained so far.

Only two, $|V_{ud}|$ and $|V_{us}|$, out of nine CKM matrix elements, are measured with an uncertainty smaller than 10%. Being input parameters to the Standard Model, it is important for the global understanding of the theory that the precision on their measurements increases. The aim is to be able to measure all the CKM elements independently and with high precision, and with them test the overall consistency.

2.1.2 CKM matrix and CP Violation

In the framework of the Standard Model, not all nine elements of the CKM matrix are independent. In general, an $N \times N$ unitary matrix has N^2 independent real parameters, $N(N-1)/2$ of which are Euler-type angles and $N(N+1)/2$ are complex phases. In the CKM matrix not all of these parameters are physically meaningful, because, for N quark generations, $2N-1$ phases can be absorbed by the freedom to select the phases of the quark fields. The number of physical parameters is therefore $N^2 - (2N-1) = (N-1)^2$, with $(N-1)(N-2)/2$ complex phases. In the case of $N=3$ families, as in the Standard Model, only four independent parameters are left, three angles and a single complex phase.

The unitarity condition, which is expressed by the orthonormality of the rows and columns of the matrix,

$$\sum_i |V_{i\alpha}|^2 = 1, \quad \sum_i V_{i\alpha} V_{i\beta}^* = 0, \quad (2.4)$$

could, in principle, be used to determine the whole matrix once four elements are known. The constraints are such that even a small relative uncertainty in one of the large (and easiest to measure) quantities, completely dominates the smaller elements, rendering such a determination impossible. For this reason, a complete determination of the matrix requires the measurement of some of the smallest elements. These elements are the ones which are measured in processes involving B physics.

The complex phase appearing in the CKM matrix introduces CP violation in the Standard Model (it is also necessary that all quarks of the same charge have different masses [24]). The matrix elements can be parameterized as a function of four independent parameters in many manners. One of the most commonly used is due to Wolfenstein [25], with a generalization to include higher order corrections first presented in Ref. [26]

$$\begin{pmatrix} V_{ud} & V_{us} & V_{ub} \\ V_{cd} & V_{cs} & V_{cb} \\ V_{td} & V_{ts} & V_{tb} \end{pmatrix} = \begin{pmatrix} 1 - \lambda^2/2 & \lambda & A\lambda^3(\rho - i\eta) \\ -\lambda & 1 - \lambda^2/2 & A\lambda^2 \\ A\lambda^3(1 - \rho - i\eta) & -A\lambda^2 & 1 \end{pmatrix} + \mathcal{O}(\lambda^4). \quad (2.5)$$

In this parametrization all the matrix elements are expressed as a function of the four real parameters λ , A , ρ , and η . In order to include high order corrections, up to $\mathcal{O}(\lambda^6)$, new variables, $\bar{\rho}$ and $\bar{\eta}$, are defined as $\bar{\rho} = \rho(1 - \lambda^2/2)$ and $\bar{\eta} = \eta(1 - \lambda^2/2)$. The expression of some of the CKM matrix elements is modified by the inclusion of $\mathcal{O}(\lambda^6)$ corrections as:

$$\begin{aligned} V_{ud} &= 1 - \frac{\lambda^2}{2} & V_{cd} &= -\lambda + \frac{1}{2}A^2\lambda^5[1 - 2(\rho + i\eta)] \\ V_{cs} &= 1 - \frac{\lambda^2}{2} - \frac{1}{8}\lambda^4(1 + 4A^2) & V_{td} &= A\lambda^3(1 - \bar{\rho} - i\bar{\eta}) \\ V_{ts} &= -A\lambda^2 + \frac{1}{2}A(1 - 2\rho)\lambda^4 - i\eta A\lambda^4 & V_{tb} &= 1 - \frac{1}{2}A^2\lambda^4. \end{aligned}$$

In the parametrization in Eq. 2.5, $\eta \neq 0$ is needed to incorporate CP violation in the Standard Model, and $\lambda \sim 0.22$ is the sine of the Cabbibo angle.

Recalling the unitarity condition expressed in Eq.2.4, and applying it to first row and first column, the following equation holds

$$V_{ud}V_{ub}^* + V_{cd}V_{cb}^* + V_{td}V_{tb}^* = 0. \quad (2.6)$$

Since V_{ij} are complex numbers, this relation can be represented as a triangle in the plane of complex numbers: it is the *Unitarity Triangle*. It is customary to rescale the triangle dividing all the terms by $|V_{cd}V_{cb}^*|$, which, to a very good accuracy, $\mathcal{O}(\lambda^7)$, is real and equal to $A\lambda^3$. Therefore the triangle can be drawn as in Fig. 2.1.

The values of the triangle sides can be written as

$$\begin{aligned} \overline{CA} &\equiv \frac{|V_{ud}V_{ub}^*|}{|V_{cd}V_{cb}^*|} = \sqrt{\bar{\rho}^2 + \bar{\eta}^2} = \left(1 - \frac{\lambda^2}{2}\right) \frac{1}{\lambda} \left| \frac{V_{ub}}{V_{cb}} \right|, \quad \text{and} \\ \overline{BA} &\equiv \frac{|V_{td}V_{tb}^*|}{|V_{cd}V_{cb}^*|} = \sqrt{(1 - \bar{\rho})^2 + \bar{\eta}^2} = \frac{1}{\lambda} \left| \frac{V_{td}}{V_{cb}} \right|. \end{aligned} \quad (2.7)$$

A precise measurement of the sides of the triangle, through the measurement of the CKM matrix elements, verifying that they really form a triangle would constitute a very important test of the Standard Model and of the understanding of the CP violation mechanism. Furthermore, the angles α , β , and γ of the triangle are also experimentally accessible. Any significant

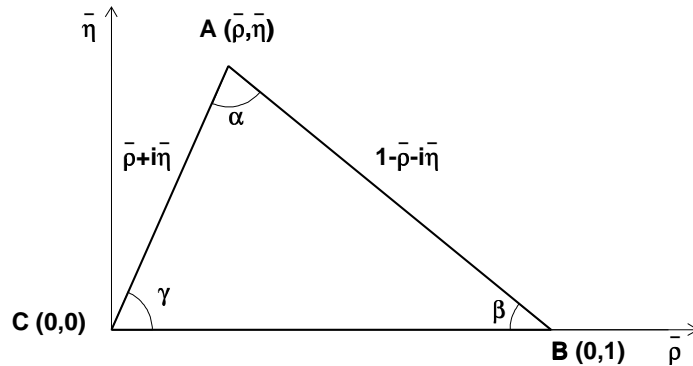


Figure 2.1: Unitarity triangle in the complex $(\bar{\rho}, \bar{\eta})$ plane.

inconsistency between all these measurements would indicate the presence of physics beyond the Standard Model. Completing the picture shown above is today one of the most active domains in particle physics.

2.2 Phenomenology of B mixing and oscillations

Particle anti-particle mixing was first observed and studied in the neutral kaon system [27] in the fifties. It is a phenomenon which has always been of fundamental importance for testing the Standard Model and suggesting extensions to it. Being a FCNC process it involves heavy quark loops and consequently it is a perfect testing ground for heavy flavour physics: from the calculation of the $K_L^0 - K_S^0$ mass difference, the value of the charm quark mass was estimated before its discovery [28], for instance.

Two neutral B-mesons exhibit the phenomenon of mixing; these are $B_d = (\bar{b}d)$ and $B_s = (\bar{b}s)$. Hereafter they are generically denoted B_q . A B_q meson can be produced in either of the two flavour-eigenstates $|B_q\rangle = |(\bar{b}q)\rangle$ or $|\bar{B}_q\rangle = |(b\bar{q})\rangle$. Due to electroweak flavour-changing interactions, this initial state evolves into a time-dependent quantum superposition of the two flavour states as $a(t)|B_q\rangle + b(t)|\bar{B}_q\rangle$, which satisfies the equation

$$i\frac{\partial}{\partial t} \begin{pmatrix} a(t) \\ b(t) \end{pmatrix} = \mathcal{H}_{\text{eff}} \begin{pmatrix} a(t) \\ b(t) \end{pmatrix} \quad \text{with} \quad \mathcal{H}_{\text{eff}} = M - i\frac{\Gamma}{2}, \quad (2.8)$$

where \mathcal{H}_{eff} is the effective Hamiltonian. The operators M and Γ describe the dispersive and absorptive parts of the $B_q - \bar{B}_q$ mixing, they are called *mass* and *decay* matrices. The B-meson is not a stable particle, and therefore \mathcal{H}_{eff} , which does not include the decay products, can not be hermitian. The matrices M and Γ instead, are hermitian, and, because of CPT invariance, their diagonal elements are equal: they represent the mass M_{B_q} and width Γ_{B_q} of the B_q and \bar{B}_q flavour states. The effective Hamiltonian can therefore be written as

$$\mathcal{H}_{\text{eff}} = \begin{pmatrix} M_{B_q} & M_{12} \\ M_{12}^* & M_{B_q} \end{pmatrix} - \frac{i}{2} \begin{pmatrix} \Gamma_{B_q} & \Gamma_{12} \\ \Gamma_{12}^* & \Gamma_{B_q} \end{pmatrix}. \quad (2.9)$$

The diagonalization of the effective Hamiltonian gives the two mass eigenstates

$$|B_{1,2}\rangle = p|B_q\rangle \pm q|\bar{B}_q\rangle, \quad (2.10)$$

and the corresponding eigenvalues

$$\lambda_{1,2} = \left(M_{B_q} - \frac{i}{2}\Gamma_{B_q} \right) \pm \frac{q}{p} \left(M_{12} - \frac{i}{2}\Gamma_{12} \right). \quad (2.11)$$

In the above equations two complex coefficients q and p have been introduced, they are defined as

$$\frac{q}{p} = \sqrt{\frac{M_{12}^* - i\Gamma_{12}^*/2}{M_{12} - i\Gamma_{12}/2}}, \quad \text{with} \quad |q|^2 + |p|^2 = 1. \quad (2.12)$$

The time dependence of these eigenstates of well-defined masses $M_{1,2} = \text{Re}(\lambda_{1,2})$ and widths $\Gamma_{1,2} = -2\text{Im}(\lambda_{1,2})$ is given by the phases $e^{-i\lambda_{1,2}t}$. Correspondingly, the time-evolution of pure states is given by

$$\begin{aligned} |B_q(t)\rangle &= g_1(t)|B_q(0)\rangle + \frac{q}{p}g_2(t)|\bar{B}_q(0)\rangle, \quad \text{and} \\ |\bar{B}_q(t)\rangle &= g_1(t)|\bar{B}_q(0)\rangle + \frac{p}{q}g_2(t)|B_q(0)\rangle, \end{aligned} \quad (2.13)$$

where

$$g_{1,2} = \frac{1}{2} \left(e^{-i\lambda_1 t} \pm e^{-i\lambda_2 t} \right). \quad (2.14)$$

The above equations mean that the flavour states oscillate into each other with time-dependent probabilities:

$$\begin{aligned} \mathcal{P}_{B_q \rightarrow B_q}(t) &= N \frac{e^{-\Gamma_{B_q} t}}{2} \left[\cosh\left(\frac{\Delta\Gamma_{B_q} t}{2}\right) \pm \cos(\Delta M_{B_q} t) \right], \quad \text{and} \\ \mathcal{P}_{B_q \rightarrow \bar{B}_q}(t) &= N \left| \frac{q}{p} \right|^2 \frac{e^{-\Gamma_{B_q} t}}{2} \left[\cosh\left(\frac{\Delta\Gamma_{B_q} t}{2}\right) \pm \cos(\Delta M_{B_q} t) \right], \end{aligned} \quad (2.15)$$

where

$$\Delta M_{B_q} = |M_1 - M_2|, \quad \Delta\Gamma_{B_q} = |\Gamma_1 - \Gamma_2|, \quad (2.16)$$

and N is the normalization factor defined by

$$\int_0^\infty dt \left[\mathcal{P}_{B_q \rightarrow B_q}(t) + \mathcal{P}_{B_q \rightarrow \bar{B}_q}(t) \right] = 1. \quad (2.17)$$

Approximations

Two approximations can be taken to simplify the formulae shown above which still give expressions precise enough for the purpose of the experimental testing.

1. CP conservation in mixing

CP conservation implies (Eqs. 2.12, 2.13, 2.14)

$$\begin{aligned} \langle B_q | M | \bar{B}_q \rangle &= \langle \bar{B}_q | M | B_q \rangle & \text{and therefore} & & M_{12} &= & M_{12}^* , \\ \langle B_q | \Gamma | \bar{B}_q \rangle &= \langle \bar{B}_q | \Gamma | B_q \rangle & \text{and therefore} & & \Gamma_{12} &= & \Gamma_{12}^* , \end{aligned} \quad (2.18)$$

so the matrix elements M_{12} and Γ_{12} are real. Furthermore, it can also be shown that

$$p = q, \quad \Delta M_{B_q} = 2M_{12}, \quad \text{and} \quad \Delta \Gamma_{B_q} = 2\Gamma_{12}. \quad (2.19)$$

2. Negligible lifetime difference

In the approximation of negligible CP violation in the mixing process, the ratio between the width and the mass differences, $\Delta \Gamma_{B_q} / \Delta m_{B_q}$, is equal to Γ_{12} / M_{12} . In the Standard Model, this quantity is expected to be of the order of the ratio m_b^2 / m_t^2 . It is therefore a small quantity, and the same for the two neutral B meson systems. It can be calculated with lattice QCD, with typical results $\sim 5 \times 10^{-3}$. The width difference, $\Delta \Gamma_{B_q}$, is caused by the existence of final states to which both the B_q and \bar{B}_q mesons can decay. Such decays involve $b \rightarrow c\bar{c}q$ quark-level transitions, which are Cabbibo-suppressed if $q = d$ and Cabbibo-allowed if $q = s$. Standard Model computations thus predict $\Delta \Gamma / \Gamma$ to be very small for the B_d system (below 1% [13]) and somewhat higher for the B_s system, up to $\sim 20\%$. Experimental results show $\Delta \Gamma_{B_s} / \Gamma_{B_s} = 0.16_{-0.09}^{+0.08}$ [29]. There is no experimental constraint for $\Delta \Gamma_{B_d} / \Gamma_{B_d}$. Neglecting $\Delta \Gamma_{B_q}$ in Eq. 2.15 means replacing the hyperbolic cosine by unity. Even for the B_s system, this approximation is reasonable and is used along this thesis.

With the approximations above, the time dependent probabilities of Eq. 2.15 become

$$\begin{aligned} \mathcal{P}_{B_q \rightarrow B_q}(t) &= \Gamma_{B_q} \frac{e^{-\Gamma_{B_q} t}}{2} [1 + \cos(\Delta m_{B_q} t)] , \\ \mathcal{P}_{B_q \rightarrow \bar{B}_q}(t) &= \Gamma_{B_q} \frac{e^{-\Gamma_{B_q} t}}{2} [1 - \cos(\Delta m_{B_q} t)] , \end{aligned} \quad (2.20)$$

which are the expressions used along this thesis. The probability density function for a B_q (\bar{B}_q) is therefore the exponential decay modulated by a cosine of frequency Δm_{B_q} , the mass difference between the two mass eigenstates. In Eq. 2.20, the convention $\hbar = 1$, $c = 1$ is taken, and consequently Δm_{B_q} is expressed in units of inverse time. The conversion factor between ps^{-1} and eV/c^2 is $1 \text{ ps}^{-1} \simeq 6.6 \times 10^{-4} \text{ eV}/c^2$. The mass difference Δm_{B_q} is always expressed in ps^{-1} in this thesis.

2.2.1 B mixing and the CKM matrix

In the framework of the Standard Model, neutral B-meson mixing is only possible at the one (or more) loop level, via Feynman *box-diagrams* involving up-type quark exchange. Two such interfering diagrams, shown in Fig. 2.2, are involved.

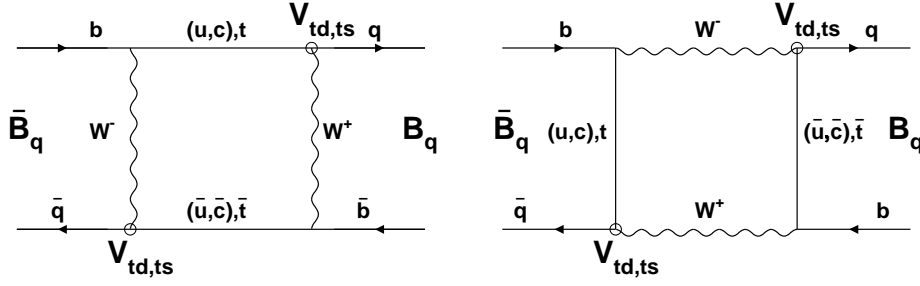


Figure 2.2: Feynman diagrams for B mixing.

The off-diagonal term of the mass matrix, $M_{12}^{(q)}$, can be determined from the computation of these diagrams. And therefore, recalling Eq. 2.19, the mass difference, Δm_{B_q} between the two neutral B-meson mass eigenstates is obtained as well. These diagrams are proportional to the square of the CKM matrix elements involved, $|V_{ib}V_{iq}|^2$, where $i = u, c, t$, and to the squared mass of the up-type quark in the internal loop. Using the parametrization of Eq. 2.5, all three terms involving CKM matrix elements are found to be of similar size for $q = d$. In the case of $q = s$, the differences between the CKM terms are not big enough to be relevant either. The quark masses are highly hierarchical, *i.e.*, $m_t \gg m_c \gg m_u$. As a consequence, the computation of these diagrams is completely dominated by the top-quark exchange. The basic equation to be solved is

$$2m_{B_q}|M_{12}^{(q)}| = |\langle \bar{B}_q | \mathcal{H}_{\text{eff}}^{(\Delta B=2)} | B_q \rangle|, \quad (2.21)$$

where $\mathcal{H}_{\text{eff}}^{(\Delta B=2)}$, relevant for scales $\mu_b = \mathcal{O}(m_b)$, is the effective Hamiltonian for a change in two units of the beauty quantum number. This Hamiltonian can be expressed as [30]

$$\mathcal{H}_{\text{eff}}^{(\Delta B=2)} = \frac{G_F^2}{16\pi^2} M_W^2 |V_{tq}V_{tb}^*|^2 S(x_t) C(\mu_b) \hat{Q}(\mu_b)^{(\Delta B=2)} + h.c. \quad (2.22)$$

Where G_F is the Fermi constant, M_W is the W-boson mass, $x_t = m_t^2/M_W^2$, $S(x)$, the Inami-Lim function reads [31]

$$S(x) = x \left[\frac{1}{4} + \frac{9}{4} \frac{1}{(1-x)} - \frac{3}{2} \frac{1}{(1-x)^2} - \frac{3}{2} \frac{x^2 \ln x}{(1-x)^3} \right], \quad (2.23)$$

and can be approximated with $0.784x^{0.76}$. The function $C(\mu_b)$ and the operator $\hat{Q}(\mu_b)$ include all the QCD corrections, *i.e.*, the computation of internal quark and gluon loops. The study of B-mixing from a theoretical point of view involves strong interactions at two distinct energy scales. The electroweak scale, of order M_W , and the quark confinement scale, of order Λ_{QCD} . In the first case, perturbative QCD techniques can be applied, to obtain $C(\mu_b)$. Non-perturbative QCD is used to get an estimate of the matrix element $|\langle \bar{B}_q | \hat{Q}(\mu_b) | B_q \rangle|$ [14, 30]. The dependence on the energy scale μ_b disappears when both QCD terms are computed.

The expression for Δm_{B_q} is obtained from Eq. 2.21 and Eq. 2.22, and can be written as [14]

$$\Delta m_{B_q} = \frac{G_F^2}{6\pi^2} M_W^2 m_{B_q} |V_{tq}V_{tb}^*|^2 S(x_t) \eta_B B_{B_q} F_{B_q}^2. \quad (2.24)$$

The factor η_B stands for the perturbative QCD corrections. It has been evaluated to be $\eta_B = 0.55 \pm 0.01$ and it is the same for the B_d and B_s systems: short distance QCD calculations do not depend on the light quark in the B-meson [32]. The uncertainty on its estimate comes from the uncertainty on the top-quark mass and from the fact that the calculation is done only up to the next-to-leading order. The term B_{B_q} is called the *Bag*-parameter, it measures deviations from the vacuum saturation approximation [33] which consists in ignoring gluon exchanges between B_q and \bar{B}_q quarks. This approximation would correspond to $B_{B_q} = 1$. The last term, F_{B_q} , is the leptonic decay constant defined by the expression [34]

$$\langle 0 | \bar{b} \gamma_\mu \gamma_5 q | B_q(p) \rangle = i p_\mu F_{B_q} . \quad (2.25)$$

Both these non-perturbative QCD quantities are computed using lattice QCD. A vast literature on these calculations is available with slightly different results depending on the approach followed. The ‘‘average’’ values quoted in Ref. [35], for instance, for the decay constants are

$$F_{B_d} = (200 \pm 40) \text{ MeV} , \quad F_{B_s} = (230 \pm 40) \text{ MeV} , \quad \text{and} \quad \frac{F_{B_s}}{F_{B_d}} = 1.15 \pm 0.07 . \quad (2.26)$$

In the same reference, the value given for the *Bag*-parameter does not distinguish $q = d$ from $q = s$ (although it is done in other references like [34]) because all methods used for the *Bag*-parameter estimate predict B_{B_s}/B_{B_d} very close to one. The values quoted in Ref. [35] are

$$B_{B_q}(m_b) = 0.91 \pm 0.06 , \quad \text{and} \quad \frac{B_{B_s}}{B_{B_d}} = 1.00 \pm 0.03 , \quad (2.27)$$

The mass difference Δm_{B_q} is an experimentally accessible parameter. Indeed, from Eq. 2.20 it can be interpreted as the B_q -meson oscillation frequency. As seen in Eq. 2.24, Δm_d and Δm_s are directly related to CKM matrix elements. Their measurement, modulo theoretical calculations, would allow poorly known terms of the CKM matrix to be determined and the matrix properties to be tested. However, the theoretical uncertainties are, for the time being, too large to give relevant constraints on the CKM matrix elements involved. Nevertheless, if the ratio of the mass differences of the two neutral B-meson systems is taken, the dependences on m_t and some QCD corrections cancel out, and the following expression is obtained

$$\frac{\Delta m_s}{\Delta m_d} = \frac{m_{B_s}}{m_{B_d}} \xi^2 \left| \frac{V_{ts}}{V_{td}} \right|^2 , \quad (2.28)$$

where all the theoretical uncertainties are contained in the parameter ξ ,

$$\xi \equiv \frac{F_{B_s} \sqrt{B_{B_s}}}{F_{B_d} \sqrt{B_{B_d}}} . \quad (2.29)$$

From Eq. 2.26, the decay constants have $\sim 20\%$ uncertainty, whereas their ratio, F_{B_s}/F_{B_d} , is better understood from a theoretical point of view, with only 7% uncertainty. As a consequence, the theoretical uncertainties on the parameter ξ are also under control, with a present best value of $\xi = 1.15 \pm 0.07$ [35]. Therefore, if both Δm_d and Δm_s were measured, the quantity $|V_{ts}|/|V_{td}|$ could be determined with small theoretical uncertainties from their ratio. Getting a measurement of $|V_{ts}|/|V_{td}|$ is one of the main motivations for pursuing a measurement of the Δm_s parameter.

2.2.2 B mixing and CP violation

A measurement of both Δm_d and Δm_s would have an important impact on the understanding of CP violation in the Standard Model. From Eq. 2.7 and Eq. 2.28, one of the sides of the unitarity triangle (Fig. 2.1) can be expressed as

$$\overline{BA} = \frac{1}{\lambda} \left| \frac{V_{td}}{V_{cb}} \right| = \frac{1}{\lambda} \left| \frac{V_{td}}{V_{ts}} \right| \left| \frac{V_{ts}}{V_{cb}} \right| = \frac{1}{\lambda} \sqrt{\frac{m_{B_s} \Delta m_d}{m_{B_d} \Delta m_s}} \xi \left| \frac{V_{ts}}{V_{cb}} \right|. \quad (2.30)$$

The CKM matrix elements $|V_{ts}|$ and $|V_{cb}|$ are, to a very good approximation, $\mathcal{O}(\lambda^4)$, equal. Therefore, from Eq. 2.30, the measurement of both neutral B-meson systems oscillation frequencies is directly related to one of the sides of the unitarity triangle. Part of the CP violation description in the Standard Model can thus be obtained from the experimental results on Δm_d and Δm_s .

The values of the parameters $\bar{\rho}$ and $\bar{\eta}$, from the unitarity triangle, can be extracted from a global fit to a particular set of experimental measurements and theoretical computations [36]. The list of inputs to this global fit is: Δm_d , Δm_s , $|V_{ub}|$, $|V_{cb}|$, m_t , $|\varepsilon_K|$ (from CP violation measurements in the kaon system), B_K (the *Bag*-parameter for the kaon system), $F_{B_d} \sqrt{B_{B_d}}$, and ξ . The results presented in Ref. [36]:

$$\bar{\rho} = 0.224 \pm 0.038 \quad \bar{\eta} = 0.317 \pm 0.040 \quad \sin(2\beta) = 0.698 \pm 0.066 \quad (2.31)$$

are compatible with the first direct measurements of the angle β of the unitarity triangle at the asymmetric B factories. An average of the preliminary results reads, $\sin(2\beta) = 0.48 \pm 0.16$ [37].

If the experimental input on B_s oscillations is removed from the global CKM matrix fit described above, constraints on the still unmeasured oscillation frequency for B_s mesons can be obtained. One of the many examples of such an analysis is presented in Ref. [38]. The probability density function for Δm_s obtained in that reference is shown in Fig. 2.3.

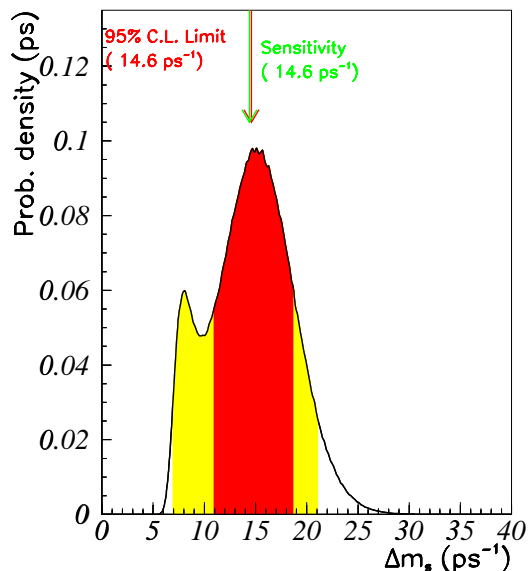


Figure 2.3: Probability density function for Δm_s .

Figure 2.3 shows that constraints on the CKM matrix elements favour a value of Δm_s around 15 ps^{-1} and values above 25 ps^{-1} would be difficult to accommodate in the absence of new physics.

2.2.3 State-of-the-art

Evidence for neutral B-meson mixing was first observed by the UA1 Collaboration at CERN, Ref. [39]. An excess of like-sign dimuon events was observed. The predicted ratio for like-sign to unlike-sign muon pairs was 0.26 ± 0.03 , coming from events where one muon arises from a B-decay and the other from a cascade charm decay. However, the measured ratio was $0.42 \pm 0.07 \pm 0.03$, which constituted the first experimental evidence for B^0 -mixing. At that time, b-production fractions were poorly known and it was therefore not possible to disentangle the contribution of B_d and of B_s mixing in the result obtained. The theoretical computations indicated already that the oscillation frequency for B_s was higher than that of B_d . Moreover, the ARGUS and CLEO [40, 41] Collaborations at Desy and CESR had, at that time, put limits on r_d , $r_d < 0.12$ at 90% C.L. and $r_d < 0.24$ at 90% C.L. respectively (r_d is related with χ_d –the mixing parameter, Section 3.1– through: $r_d = \chi_d/(1-\chi_d)$). Results from MARKII [42] were consistent with a very low value of χ_d as well. All these results together made the UA1 Collaboration favour an interpretation of their result in terms of mainly B_s mixing. However, thanks to the much more precise information presently available, it is now known that the effect measured at UA1 was dominated by B_d mixing. Few months after the UA1 publication, ARGUS [43] reported on the first direct observation of $B_d - \bar{B}_d$ mixing at the $\Upsilon(4S)$ resonance. The mass of the $\Upsilon(4S)$ is not high enough to create a $B_s - \bar{B}_s$ pair. Therefore, there is no uncertainty on the neutral B-meson composition, and no possibility of misinterpretation. The first measurement of the B_d mixing parameter at the $\Upsilon(4S)$ was obtained by the ARGUS Collaboration in 1987[43], $r_d = 0.21 \pm 0.08$, followed by a slightly more precise result from the CLEO Collaboration in 1989, $r_d = 0.19 \pm 0.06 \pm 0.06$ [44]. A direct measurement of B_d oscillations had to wait for LEP data and came some years later, in 1994, from the ALEPH Collaboration, $\Delta m_d = (0.50_{-0.06}^{+0.07} \text{ }_{-0.10}^{+0.11}) \text{ ps}^{-1}$ [45].

$B_d - \bar{B}_d$ Mixing

The measurement of B_d oscillations has today become a precision measurement. The four LEP Collaborations, SLD and CDF have published results on the subject giving an average value of $\Delta m_d = 0.486 \pm 0.015 \text{ ps}^{-1}$ [48]. The CLEO and ARGUS Collaborations have performed measurements of the mixing parameter χ_d . Their results can be combined with the measurements of Δm_d with a non-trivial procedure explained in Ref. [8]. The present world combined average is $\Delta m_d = 0.487 \pm 0.014 \text{ ps}^{-1}$ [8] (including results from LEP, SLD, CDF, ARGUS and CLEO).

The asymmetric B-factories have been running for more than a year now and the first results presented include measurements on B_d oscillations. These results are still preliminary but show that, with some more time, the precision of the world average for the B_d mixing result will further improve and will soon be dominated by the results from the Babar and Belle experiments taking data on the asymmetric B-factories.

$B_s - \bar{B}_s$ Mixing

Studies on B_s oscillations have only been possible until now at the Z resonance (LEP and SLC) and with lower sensitivity at the Tevatron. The B_s oscillation frequency is expected to be much larger than that of B_d mesons, as it can be deduced from Eq. 2.28 and Fig. 2.3. Up to now, B_s oscillations have not been resolved and only lower limits have been set. The latest world average lower limit which includes some of the results presented in this thesis is $\Delta m_s > 15 \text{ ps}^{-1}$ at 95% C.L. [50].

Some of the analyses both at SLD and at the LEP Collaborations are still expected to improve slightly. It is not excluded that the final combination of the Z peak data analyses be able to resolve B_s oscillations. If with the Z peak data only a lower limit is set, the first measurement will most probably come from the experiments at the Tevatron collider in the next years [51].

The width difference $\Delta\Gamma_s$ could be large enough to be measured before the mass difference Δm_s [52]. The theoretical estimate of $\Delta\Gamma_s/\Delta m_s$ suffers from no CKM uncertainty, it has only QCD contributions which can be computed on the lattice. Therefore, a reliable estimate of Δm_s could be inferred a the measured value of $\Delta\Gamma_s$. The present measurement of $\Delta\Gamma_s/\Gamma_s$ is however not accurate [29], and only provides a mild constraint on the allowed region for Δm_s : $\Delta m_s = 29^{+16}_{-21} \text{ ps}^{-1}$ [50].

2.3 B mixing beyond the Standard Model

In general, most of the extensions of the Standard Model which are being studied do not have sizeable implications on processes at tree level, and therefore have negligible contributions to B decays. The B-mixing phenomenon is only possible at the one (or more) loop level. Contributions from physics beyond the Standard Model can enter these loops, and therefore B-mixing can be a test bench for new theoretical models.

It is not possible in the scope of this thesis to give a comprehensive review of the possible extensions of the Standard Model which have implications on mixing parameters. A selection of examples found in the literature is given. A more extensive discussion is presented, for example, in Ref. [53].

One of the models which is being presently studied is called *extra-dimensions*. In this model the ordinary four-dimensional Standard Model arises as a low energy effective theory of models defined in five or more dimensions. One of the simplest generalizations has one single extra-dimension. The model contains fermions which live in four dimensions, and gauge bosons and one scalar doublet propagating in five dimensions [54]. This extended model allows phenomenological constraints derived from one loop processes to be extracted, and in particular some predictions related with B-mixing can be performed. The correction induced by the extra-dimension to the Inami-Lim function $S(x_t)$ has been estimated giving the range $1 < S(x_t) < 10$, while the Standard Model value is $S(x_t) \sim 2.6$. Experimentally, the value of $S(x_t)$ has still some uncertainties, which makes impossible yet to extract any bound on extra-dimension models from the B-mixing data. However, if in the future a value of $S(x_t)$ larger than that of the Standard Model is found, extra-dimensions could easily accommodate it.

Probably the most popular framework for physics beyond the Standard Model is supersymmetry. Many contributions to the $B - \bar{B}$ mixing are possible. However the parameter space of the different models is vast and firm constraints are difficult to establish. The effect of supersymmetry on $B - \bar{B}$ mixing could be very significant: for certain values of the parameters, for example, the total supersymmetric contribution to $B_d - \bar{B}_d$ mixing can be twice as large as that of the Standard Model [53].

Finally, there are theories with a real (orthogonal) CKM matrix, which therefore explain CP violation in some other means, *superweak theories* [55]. These theories require that Standard Model fits to the unitarity triangle gives $\eta = 0$. Experimental limits on B_s oscillations have now almost excluded a negative value of ρ , and in general do not favour the region $\eta = 0$ with positive ρ either. In the framework of the pure superweak theories, Δm_s is expected to be larger than in the Standard Model: between 10 ps^{-1} and 32 ps^{-1} at 95% C.L., which is still compatible with the present experimental results.

